Photomask Technology 2009

Larry S. Zurbrick
M. Warren Montgomery
Editors

14–17 September 2009
Monterey, California, United States

Sponsored by

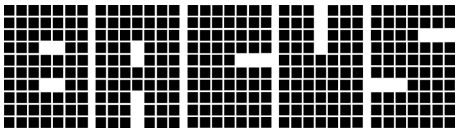

The international technical group of SPIE dedicated
to the advancement of photomask technology

Published by
SPIE

Part One of Two Parts

Volume 7488

Proceedings of SPIE, 0277-786X, v. 7122

The papers included in this volume were part of the technical conference cited on the cover and title page. Papers were selected and subject to review by the editors and conference program committee. Some conference presentations may not be available for publication. The papers published in these proceedings reflect the work and thoughts of the authors and are published herein as submitted. The publisher is not responsible for the validity of the information or for any outcomes resulting from reliance thereon.

Please use the following format to cite material from this book:
Author(s), "Title of Paper," in *Photomask Technology 2009*, edited by Larry S. Zurbrick, M. Warren Montgomery, Proceedings of SPIE Vol. 7488 (SPIE, Bellingham, WA, 2009) Article CID Number.

ISSN 0277-786X
ISBN 9780819477958

Published by
SPIE
P.O. Box 10, Bellingham, Washington 98227-0010 USA
Telephone +1 360 676 3290 (Pacific Time) · Fax +1 360 647 1445
SPIE.org

Printed in the United States of America.

Publication of record for individual papers is online in the SPIE Digital Library.

SPIEDigitalLibrary.org

Paper Numbering: Proceedings of SPIE follow an e-First publication model, with papers published first online and then in print and on CD-ROM. Papers are published as they are submitted and meet publication criteria. A unique, consistent, permanent citation identifier (CID) number is assigned to each article at the time of the first publication. Utilization of CIDs allows articles to be fully citable as soon they are published online, and connects the same identifier to all online, print, and electronic versions of the publication. SPIE uses a six-digit CID article numbering system in which:

- The first four digits correspond to the SPIE volume number.
- The last two digits indicate publication order within the volume using a Base 36 numbering system employing both numerals and letters. These two-number sets start with 00, 01, 02, 03, 04, 05, 06, 07, 08, 09, 0A, 0B … 0Z, followed by 10-1Z, 20-2Z, etc.

The CID number appears on each page of the manuscript. The complete citation is used on the first page, and an abbreviated version on subsequent pages. Numbers in the index correspond to the last two digits of the six-digit CID number.

Contents

Part One

MASK FILMS, PROCESS CONTROL, AND EQUIPMENT

NANO-IMPRINT AND PATTERNED MEDIA TECHNOLOGY II

PATTERNING TECHNOLOGY AND TOOLS

METROLOGY I

METROLOGY II

MASK CLEANING AND MAINTENANCE

NANO-IMPRINT AND PATTERNED MEDIA TECHNOLOGY III

Part Two

POSTER SESSION: OPC

POSTER SESSION: PATTERN GENERATION/EQUIPMENT

POSTER SESSION: SIMULATION AND MODELING

Conference Committee

Conference Chair

Larry S. Zurbrick, Agilent Technologies, Inc. (United States)

Conference Cochair

M. Warren Montgomery, College of NanoScale Science and Engineering (CNSE) and SEMATECH Inc. (United States)

Program Committee

Frank Abboud, Intel Corporation (United States)
Kiho Baik, Luminescent Technologies, Inc. (United States)
Artur P. Balasinski, Cypress Semiconductor Corporation (United States)
Uwe F.W. Behringer, UBC Microelectronics (Germany)
Ronald R. Bozak, RAVE LLC (United States)
William H. Broadbent, KLA-Tencor Corporation (United States)
Peter D. Buck, Toppan Photomasks, Inc. (United States)
Han-Ku Cho, SAMSUNG Electronics Company, Ltd. (Korea, Republic of)
Frank A. Driessen, Takumi Technology B.V. (Netherlands)
Roxann L. Engelstad, University of Wisconsin, Madison (United States)
Emily E. Gallagher, IBM Corporation (United States)
Brian J. Grenon, Grenon Consulting, Inc. (United States)
Naoya Hayashi, Dai Nippon Printing Company, Ltd. (Japan)
Mark T. Jee, HOYA Corporation USA (United States)
Rik M. Jonckheere, IMEC (Belgium)
Bryan S. Kasprowicz, Photronics, Inc. (United States)
Kurt R. Kimmel, Advanced Mask Technology Center GmbH & Company KG (Germany)
Chin-Hsiang Lin, Taiwan Semiconductor Manufacturing Company Ltd. (Taiwan)
Wilhelm Maurer, Infineon Technologies AG (Germany)
Thomas H. Newman, Micronic Laser Systems Inc. (United States)
Hiroshi Nozue, NuFlare Technology, Inc. (Japan)
James E. Potzick, National Institute of Standards and Technology (United States)
Emmanuel Rausa, Oerlikon USA Inc. (United States)
Frank M. Schellenberg, Mentor Graphics Corporation (United States)
Thomas Scherübl, Carl Zeiss SMS GmbH (Germany)
Robert J. Socha, ASML (United States)
Christopher A. Spence, GlobalFoundries Inc. (United States)
Wolfgang Staud, Applied Materials (United States)

Jacek K. Tyminski, Nikon Precision Inc. (United States)
J. Tracy Weed, Synopsys, Inc. (United States)
John M. Whittey, KLA-Tencor Corporation (United States)

Session Chairs

1 Invited Session
Larry S. Zurbrick, Agilent Technologies, Inc. (United States)
M. Warren Montgomery, College of NanoScale Science and Engineering (CNSE) and SEMATECH Inc. (United States)

2 Defect Inspection and Disposition
William H. Broadbent, KLA-Tencor Corporation (United States)
Wolfgang Staud, Applied Materials (United States)

3 Defect Inspection and Repair
John M. Whittey, KLA-Tencor Corporation (United States)
Ronald R. Bozak, RAVE LLC (United States)

4 Mask Films, Process Control, and Equipment
Emily E. Gallagher, IBM Corporation (United States)
Peter D. Buck, Toppan Photomasks, Inc. (United States)

5 Nano-Imprint and Patterned Media Technology I
Dan Gentry, Xyratex International Inc. (United States)
Brian J. Grenon, Grenon Consulting, Inc. (United States)

6 Nano-Imprint and Patterned Media Technology II
Peter R. Goglia, Xyratex International Inc. (United States)
Dan Gentry, Xyratex International Inc. (United States)

7 Source-Mask Optimization
Wilhelm Maurer, Infineon Technologies AG (Germany)

8 RET and OPC/ORC
Steffen F. Schulze, Mentor Graphics Corporation (United States)
Christopher A. Spence, GlobalFoundries Inc. (United States)

9 EUV Mask Substrates and Processing
Archita Sengupta, Intel Corporation (United States)
Han-Ku Cho, SAMSUNG Electronics Company, Ltd. (Korea, Republic of)

10 Patterning Technology and Tools
Thomas H. Newman, Micronic Laser Systems Inc. (United States)
Hiroshi Nozue, NuFlare Technology, Inc. (Japan)

11 Metrology I
Thomas Scherübl, Carl Zeiss SMS GmbH (Germany)
Jacek K. Tyminski, Nikon Precision Inc. (United States)

12 Metrology II
James E. Potzick, National Institute of Standards and Technology (United States)
John M. Whittey, KLA-Tencor Corporation (United States)

13 Mask Cleaning and Maintenance
Bryan S. Kasprowicz, Photronics, Inc. (United States)
Brian J. Grenon, Grenon Consulting, Inc. (United States)

14 Nano-Imprint and Patterned Media Technology III
Naoya Hayashi, Dai Nippon Printing Company, Ltd. (Japan)
Tsutomu T. Yamashita, Western Digital Corporation (United States)

15 Nano-Imprint and Patterned Media Technology IV
Dan Gentry, Xyratex International Inc. (United States)
Thomas R. Albrecht, Hitachi Global Storage Technologies, Inc. (United States)

16 Mask Business
Uwe F.W. Behringer, UBC Microelectronics (Germany)

17 Mask Data Preparation
Frank Abboud, Intel Corporation (United States)
Christopher A. Spence, GlobalFoundries Inc. (United States)

18 Simulation and Modeling
J. Tracy Weed, Synopsys, Inc. (United States)
Kiho Baik, Luminescent Technologies, Inc. (United States)

19 EUV Mask Contamination and Cleaning
Jan H. Peters, Advanced Mask Technology Center GmbH & Company KG (Germany)
Naoya Hayashi, Dai Nippon Printing Company, Ltd. (Japan)

20 EUV Mask Data Preparation and Inspection
Naoya Hayashi, Dai Nippon Printing Company, Ltd. (Japan)
Jan H. Peters, Advanced Mask Technology Center GmbH & Company KG (Germany)

21 DPL Implementation and RET Manufacturability
Robert J. Socha, ASML (United States)
David Y. Chan, SEMATECH North (United States)

Introduction

This proceedings volume contains accepted papers from the SPIE conference on Photomask Technology 2009. The conference was arranged through the Bay Area Chrome Users Society (BACUS) and held as part of the 29th International Symposium on Photomask Technology, 14–17 September 2009 in Monterey, California, USA.

This year's conference broadened its venue by including four sessions on Nano-Imprint and Patterned Media Technology. The four sessions addressed the latest work performed in template manufacturing, inspection and repair as well as overviews of patterned magnetic data storage media manufacture and challenges. The data recording media industry is moving towards lithographically patterning magnetic media in order to achieve 1Tb/sq inch bit densities. One of the leading lithography candidates to achieve these bit densities is nano-imprint lithography.

As in past years the conference covered a broad range of the latest research and ongoing issues in the photomask industry with international representation from Europe, North America, and Asia. The year that transpired since the 2008 Photomask Technology conference has been an exceptional one not only for the electronics industry but also the worlds financial and manufacturing communities as well. Although the electronics industry was faced by the greatest decline in growth on record to date, the mask making industry persisted in driving technology forward at an impressive rate as evidenced by the papers presented at this year's conference.

This year's Special Session, "Commodity or Technology? Sub-20nm Mask Making at Yet Another Crossroad" was organized by cochair M. Warren Montgomery and Wolfgang Staud. They assembled a panel of industry experts from around the world to address the issues facing the mask industry and infrastructure in light of a possible bifurcation by the industry between EUV and Nano-Imprint lithography.

I thank all of the authors, particularly the keynote speaker Dr. Michael Polcari, President and CEO of SEMATECH, for providing his insight on collaborative approaches in the mask industry so as to drive EUV mask making to production readiness. I also thank all the members of the program committee for their hard work in helping to make this year's conference a success through their efforts ranging from reviewing abstracts through chairing sessions. I owe a special thanks to my cochair M. Warren Montgomery for his help and hard work in making this year's conference a success. Our sponsors also deserve special thanks for their continued support of Photomask Technology especially this year when the norm for many elsewhere in the industry was to decrease or eliminate budgets related

to conference activities. The SPIE staff has my gratitude for their tireless efforts in organizing the conference and ensuring that things ran smoothly as well as their efforts to provide for a timely publication of these proceedings.

I hope you find the papers contained in this proceeding informative and helpful in your professional endeavors.

Larry S. Zurbrick

Thursday Special Session Schedule

Commodity or Technology? Sub-20nm Mask Making at Yet Another Crossroad*

Chairs: **M. Warren Montgomery,** College of NanoScale Science and Engineering (CNSE) and SEMATECH Inc. (United States); **Wolfgang Staud,** Applied Materials (United States)

Opening Remarks and Introduction
M. Warren Montgomery, College of NanoScale Science and Engineering (CNSE) and SEMATECH Inc. (United States); **Wolfgang Staud,** Applied Materials (United States)

Important mask technology questions were addressed:

Is it possible to reach 100% yield with low mask order volume? Can mask users and mask makers work together to reach the point where there is enough product to deliver high yield at a reasonable cost? There is a TARP (Troubled Assets Relief Program) for the banking industry; is there a TMMRP (Troubled Mask Maker Relief Program) for the mask maker? These and other exciting topics were discussed by some of the mask industries best and brightest.

Panelists:

Naoya Hayashi, Dai Nippon Printing Company, Ltd. (Japan)

Franklin D. Kalk, Toppan Photomasks, Inc. (United States)

Brian J. Grenon, Grenon Consulting, Inc. (United States)

Mark Wagner, Applied Materials, Inc. (United States)

Bruno Lafountaine, Globalfounderies (United States)

Chiang Yang, Intel Corporation (United States)

Greg Hughes, SEMATECH Inc. (United States)

Thomas R. Albrecht, Hitachi Global Storage Tech, Inc. (United States)

Chan-Uk Jeon, SAMSUNG Electronics Co., Ltd. (Korea, Republic of)

Open Discussion

* For information about the BACUS technical group go to: www.SPIE.org/BACUSHome

Comparison of Lithographic Performance between MoSi Binary mask and MoSi Attenuated PSM.

Mitsuharu Yamana[1], Matthew Lamantia[2],Vicky Philipsen[3], Shingo Wada[1],
Tatsuya Nagatomo[1], and Yoji Tonooka[1]
[1]Toppan Printing Co., Ltd., 7-21-33 Nobidome, Niiza-shi, Saitama 352-8562, Japan
[2]Toppan Photomasks Inc (USA), Kapeldreef 75 B-3001 Leuven, Belgium
[3]IMEC vzw, Kapeldreef 75 B-3001 Leuven, Belgium
Phone: +81-48-482-4828 FAX:+81-48-481-3672 e-mail:mitsuharu.yamana@toppan.co.jp

ABSTRACT

The mask error budget continues to shrink with shrinking DRAM half pitch and MPU gate size year by year. The ITRS roadmap calls for mask CDU to be cut in half by 2014[1]. Both mask maker and mask user must take advantage of various mask properties, OPC strategies and resolution enhancement techniques to drive improvements. Mask material selection impacts both lithographic performance and mask manufacturability. In turn mask material properties and manufacturing techniques impact our ability to meet the technology roadmap. Studies have shown the advantages of polarized light[2,3] as well as the impact of various mask materials on high NA lithography[4]. In this paper we select the recently introduced binary mask material made from a MoSi absorber called Opaque MoSi On Glass (OMOG) for comparison with the conventional 6% att. PSM and 20% att. MoSi PSM. Through simulation and wafer prints, we optimized mask feature from viewpoint of MEEF and maximum exposure latitude (EL). The MoSi att. PSMs suffer from higher MEEF, which is attributed to the negative effect of TE polarization for mask duty cycle of 50% for 50 nm half pitch and below. Therefore a lower mask duty cycle is required for att. PSM to bring the MEEF performance back to acceptable levels. Experimental results confirm simulation results. As a result of the lower mask duty cycle, the att. MoSi PSMs exhibit poor Sub Resolution Assist Feature (SRAF) printability. On the contrary, the MoSi binary mask delivers both acceptable MEEF and acceptable SRAF printing performance. Moreover, we found that the mask structure impact of OMOG to wafer CD is smallest among three masks. OMOG gives the best combination of lithographic performance and delivery compared to the MoSi att. PSMs.

Keywords: MoSi binary mask, OMOG, 6% attenuated PSM, 20% attenuated PSM, Double patterning

1. INTRODUCTION

Since the introduction of 193nm lithography, the 6% att. PSM mask has been the standard material for critical layers. Now with the development phase for 32nm and 22nm nodes well underway, we see that lithography conditions are much different from the initial introduction of 193nm lithography. The increase in NA, the adoption of immersion lithography and the use of polarized light make it interesting and meaningful to compare lithographic performance between binary and att. PSM masks.

MoSi binary mask called Opaque MoSi On Glass (OMOG) has been developed [5]. A thin Cr is used as a hard mask to minimize loading effects[5]. The thin hard mask enables us to reduce resist thickness. This in turn improves resolution capability. Moreover it was reported that exposure latitude (EL) and MEEF of OMOG was better than Cr binary mask[5]. Then OMOG was focused as a binary mask. In addition to the OMOG (binary) and 6% att. PSM, we also evaluated a 20% att. PSM to investigate the impact of att. PSM transmission on lithographic performance.

Lithographic performance of OMOG, 6% att. PSM and 20% att. PSM in both bright field and dark field was simulated. Firstly we optimized mask feature at minimum pitch from viewpoint of maximum EL and Mask Error Enhancement Factor (MEEF). The resulting optimized mask features were different among three masks. We believe that the observed differences in optimal mask bias between materials are attributed to the differences in the degree of polarization induced by each material.

Generally, Sub Resolution Assist Feature (SRAF) use is an indispensable technique to provide adequate depth of focus (DOF) for larger pitches on layers with lithography settings that are optimized for denser pitches. But SRAF width will

Photomask and Next-Generation Lithography Mask Technology XVI, edited by Kunihiro Hosono
Proc. of SPIE Vol. 7379, 73791L · © 2009 SPIE · CCC code: 0277-786X/09/$18 · doi: 10.1117/12.824298

be critical issue with shrinking design rule. Next we investigated the impact of the optimized mask feature size on through pitch performance that includes the use of SRAF. SRAF printability between materials and across various pitches through simulation and experimental wafer results were compared. Wafer CD error was estimated to decide which mask was best. Finally, mask cycle time to further differentiate the mask materials were compared.

2. SIMULATION AND EXPERIMENTAL CONDITION

Lithographic performance of line and space such as MEEF, maximum EL and depth of focus (DOF) was calculated with rigorous simulation. Prolith version 11 (KLA Tencor) using Maxwell Simulation Mode and a 3D mask structure was selected for all simulations. Structures from half pitch (hp) 60 nm to hp 22 nm were simulated. Table 1 summarizes the lithographic condition of each hp.

hp(nm)	60	50	45	40	38	38	32	22
Exposure Method	Single Exposure						Double Patterning	
Actual hp(nm)	60	50	45	40	38	38	64	44
NA	1.2	1.35					1.1	1.35
Illumination	Annular	cQuad				Dipole	Annular	cQuad
Outer σ	0.85	0.85	0.85	0.98	0.98	0.98	0.85	0.98
Inner σ	0.65	0.65	0.65	0.81	0.81	0.83	0.65	0.81
Blade Angle(°)		30	20	20	20	40		20

Table 1. Exposure method and optical conditions.

NA was increasing with shrinking hp. An annular illumination type was selected for hp 60nm. However, cQuad illumination was selected for 50nm hp and below to obtain higher resolution capability. As for hp 38nm, dipole illumination setting was also used because hp 38nm was considered to be severe for single exposure. CD target on wafer was basically equal to hp. Generally resolution limitation was defined in Equation (1)[6];

$$\text{Resolution Limit} = \lambda / 4\text{NA} = \text{hp } 35.7 \text{ nm} \quad (1)$$

Based on Eq. 1, the resolution limit is 35.7nm hp when λ is 193nm and NA is 1.35. Therefore double pattering is required to achieve hp 32nm and hp 22nm. The final target pitch is doubled for each lithography step in double patterning. Thus, the actual half pitch is two times larger than each hp. Wafer target CD was also optimized. Final target wafer CD could be achieved through etch slimming in bright field and certain shrinking techniques in dark field[7,8] . MEEF, EL, and DOF were simulated. EL and DOF were calculated based on ±10% CD variations.

SRAF width for isolated patterns was evaluated. Isolated pattern was defined as follows;

$$\text{Isolated pitch} = (\text{Anchor pattern pitch} + 10 \text{ nm}) \times 5 \quad (2)$$

Anchor pattern is the dense line and space pattern for each hp. Two SRAFs were placed beside main pattern. The pitch between main pattern and SRAF and the pitch between the two SRAFs was the anchor pattern pitch plus 10nm. Target wafer CD was hp plus 10nm in dark filed. This takes into consideration the CD shift between resist CD and etch CD. The large as possible SRAF that show good printing performance was chosen. SRAF printability was evaluated over a CD±15% process window. The DOF of the isolated pattern was compared for each material. Next we estimated CD error on wafer. We assumed ±1% as exposure dose variation and ±2 nm as mask global CD error and quartz depth variation. Finally, the impact of mask quartz depth variations on printed CD was also simulated. Experiments to confirm the simulation results were run using the ASML XT:1900i for both hp 45nm and hp 40nm conditions. Optical conditions were matched with simulation settings. MEEF and maximum EL between experiment and simulation was compared. SRAF printability was also demonstrated experimentally. SRAF rule is shows in table 2.

Pitch Range (nm)	SRAFs	Selected Pitches (nm)
Minumum Pitch	No	90
Mid Range	No	100-150
Mid Range	Yes	180-190
200's	Yes	240-270
400's	Yes	400-480

Table 2. Pitch ranges for through pitch evaluation.

3. SIMULATION RESULTS

3.1 Maximum EL and MEEF of hp 45nm

At first we optimized mask feature from the viewpoint of maximum EL and MEEF. Figure 1 shows the maximum EL and MEEF as a function of mask feature (x1) for 45nm hp. For bright field features the flat part of the OMOG MEEF curve extends just beyond a 45nm mask feature or 50% duty cycle (DC). The OMOG maximum EL peak occurs beyond this point of the steeper part of the MEEF curve. Thus, we selected an optimized mask feature around 50% duty cycle for OMOG which occurs on the flat part of the MEEF curve. The flat part of the PSM MEEF curve occurs at a lower duty cycle. Here we choose 35nm mask feature for the 6% att. PSM and a 30nm mask feature for the 20% att. PSM respectively.

The tendency of dark field is the reverse of bright field. Again we find that a 45nm mask feature is optimal for OMOG while a 55nm mask feature is optimal for the 6% and 20% PSM masks. Table 3 contains a summary of the optimized mask features used in our simulations.

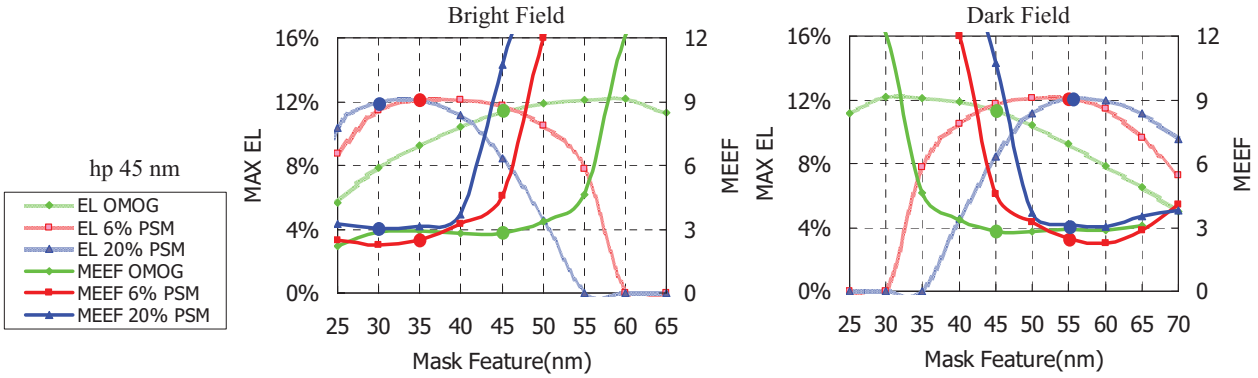

Figure 1 Maximum exposure latitude and MEEF as a function of mask feature size: dots represent optimized mask feature.

	OMOG	6% PSM	20% PSM
Bright Field	45	35	30
Dark Field	45	55	55

Table 3. Optimized mask feature size (nm).

3.2 Degree of polarization

Polarized illumination leads to an increase in contrast for hyper-NA immersion lithography[3]. All the components within the optical path, including the mask, must be compatible with this resolution enhancement technique. In order to explain the reason why the optimized mask features are different among three masks, the degree of polarization (DOP) was simulated. DOP is defined as follows:

$$DOP = (I_{TE} - I_{TM})/(I_{TE} + I_{TM}) \quad (3)$$

Figure 2 shows DOP through mask feature for the OMOG and PSM masks. The more positive DOP the larger amount of TE polarized light. Conversely the more negative the DOP the larger amount of TM polarized light. TE polarized light is preferred over TM polarized light for imaging[9]. OMOG has less effect on degree of polarization through mask feature then either PSM masks. The PSM masks tend to result in TM polarized light (more negative DOP). For the PSM masks, the mask feature size where 0th order DOP starts to decrease rapidly corresponds to the rapid decline predicted for maximum EL and increase in MEEF shown in Figure 1. PSMs have the effect of stronger TM polarization at higher duty cycles. This is considered to be the reason for the deterioration in EL and MEEF for the PSM higher DC for bright field.

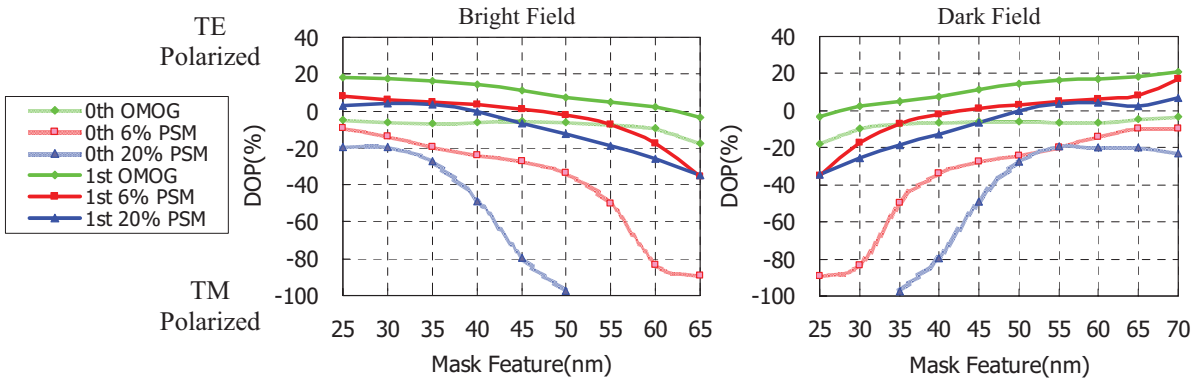

Figure 2 DOP through mask feature.

3.3 Expansion of EL and MEEF evaluation to various half pitch features.

Evaluation to different hp from 60nm to 22nm was expanded. Figure 3 shows maximum EL and MEEF through mask feature for various hp. The illumination conditions for the various half pitches are shown in Table 1.

For bright field features the optimized mask feature for OMOG shifts to higher duty cycles for the 60nm hp as shown in Figure 3. We observed similar shift away from 50% DC but in the opposite direction for the dark field features. We also see for the hp 60nm that the optimal mask feature for the 6% & 20% att. PSM shift towards lower duty cycles for bright field and higher duty cycle for dark field. The same tendency was seen for hp 50nm. As for 40nm hp and below, the optimal mask feature for OMOG is around 50% duty cycle. The optimal mask feature for 6% and 20% PSM continue to shift to small duty cycles for bright field and larger duty cycles for dark field. This trend is observed for both cQuad and dipole illumination.

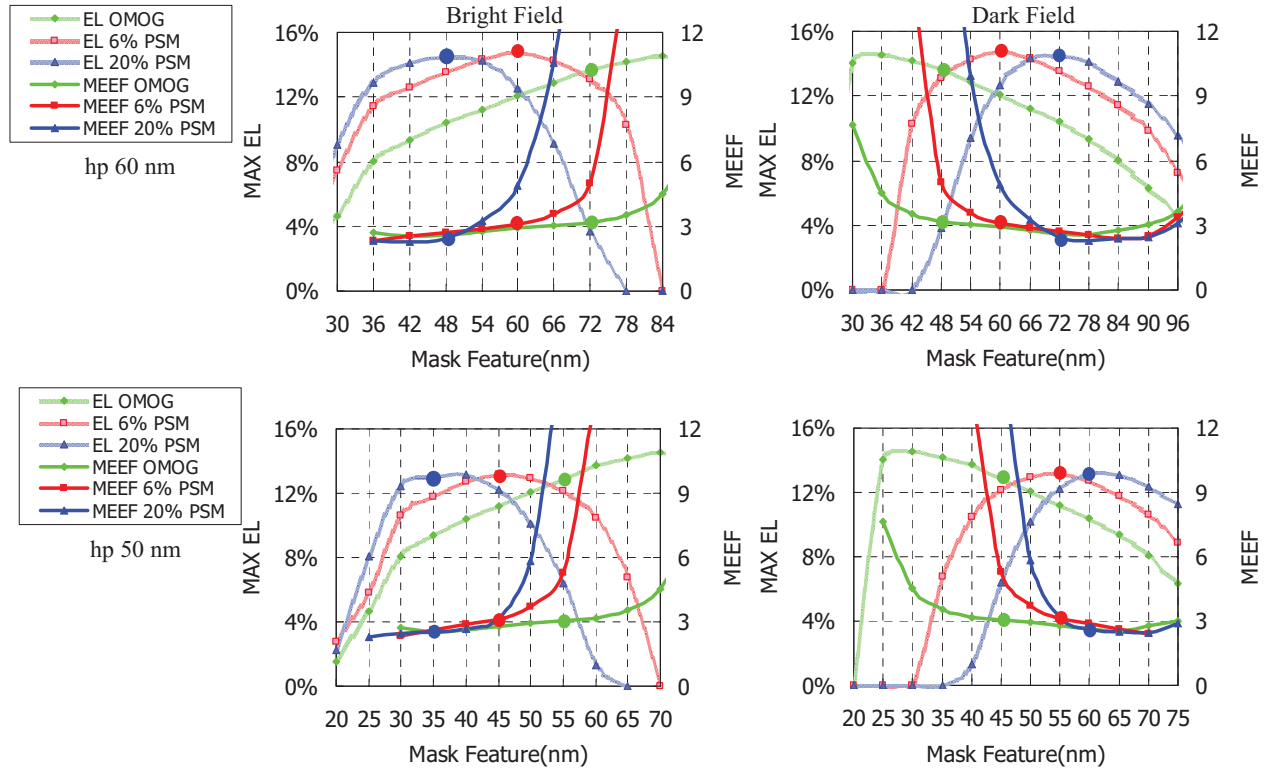

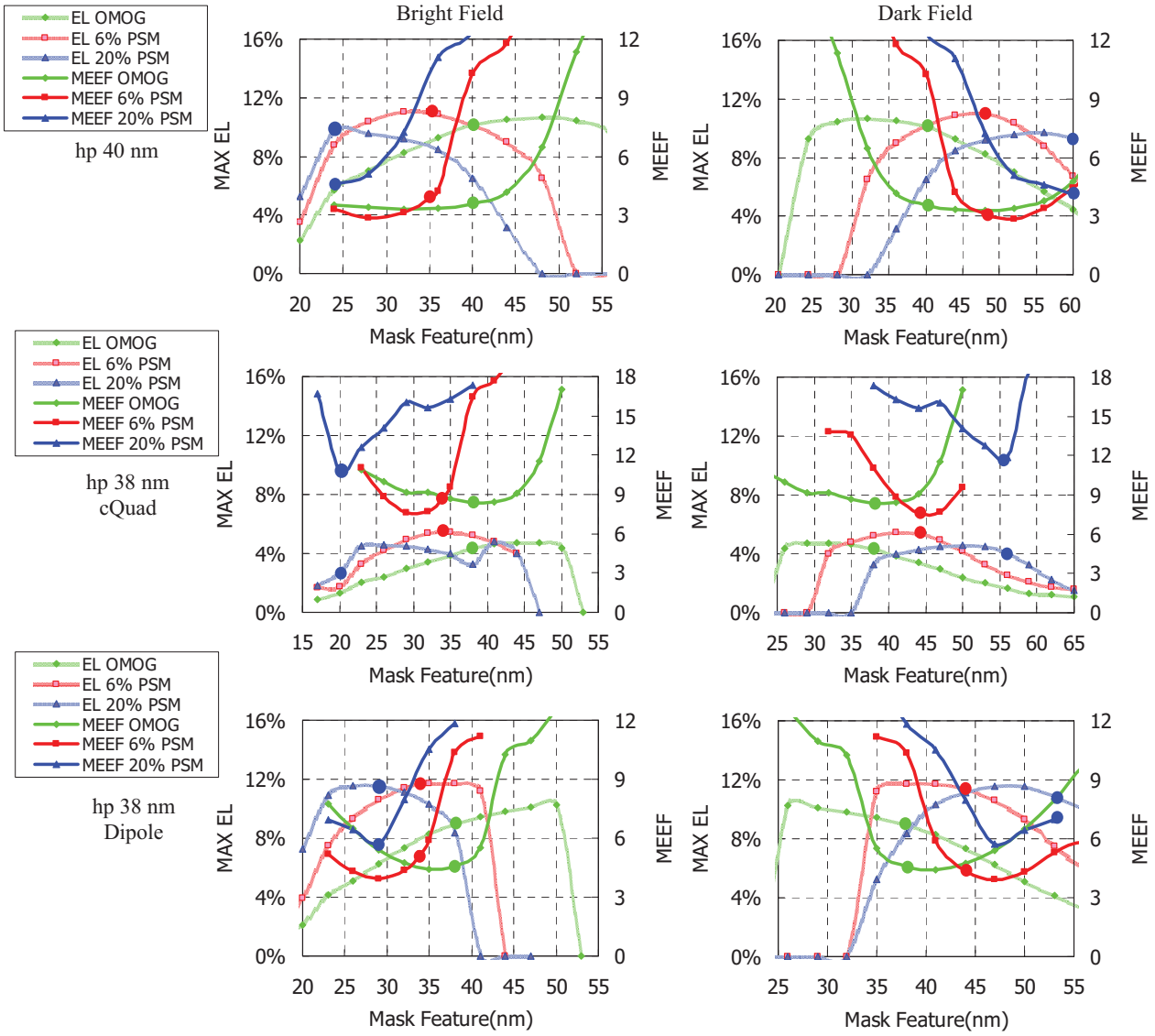

Figure 3 Maximum exposure latitude and MEEF as a function of mask feature size: dots represent optimized mask feature.

An ultimate resolution limitation is considered to be hp 35.7nm for NA1.35. We simulated lithographic performance of hp 32nm and 22nm with double patterning technique. The actual hp is 2 times larger than the final hp. But it seems to be difficult that we make CD target on wafer hp. Typically a wafer CD shrink technique such as etch slimming in bright field and shrinking in dark field can be used to adjust litho CD targets to final CD targets. We attempt to optimize both wafer CD and mask feature simultaneously. Figure 4 shows the dependence of MEEF, maximum EL and DOF on wafer CD and mask feature for the 32nm hp bright field case. The horizontal axis shows mask feature while the vertical axis shows the wafer CD. The actual pitch is 128nm. The optimum wafer CD for all masks is around 52nm because the DOF is at a maximum. The optimal mask feature was selected based on MEEF and maximum EL. Figure 5 shows dark field case. Here a 72nm wafer CD was selected for the dark field case. The optimized wafer CD in dark field is larger than that in bright field. Figure 6 shows hp 22nm bright field case. The actual pitch is 88nm. Here we see that the optimal wafer CD and mask CD are different for all three masks. For OMOG we choose a 34nm wafer CD with a 48nm mask feature. The optimum combination for 6% att. PSM is 36nm wafer CD and a 36nm mask feature. The 20% att. PSM requires a 42 nm wafer CD with a 30nm mask feature. Figure 7 shows dark field case of hp 22nm. We decided 52nm wafer CD is optimized value. We also optimized mask feature from viewpoint of MEEF and maximum EL.

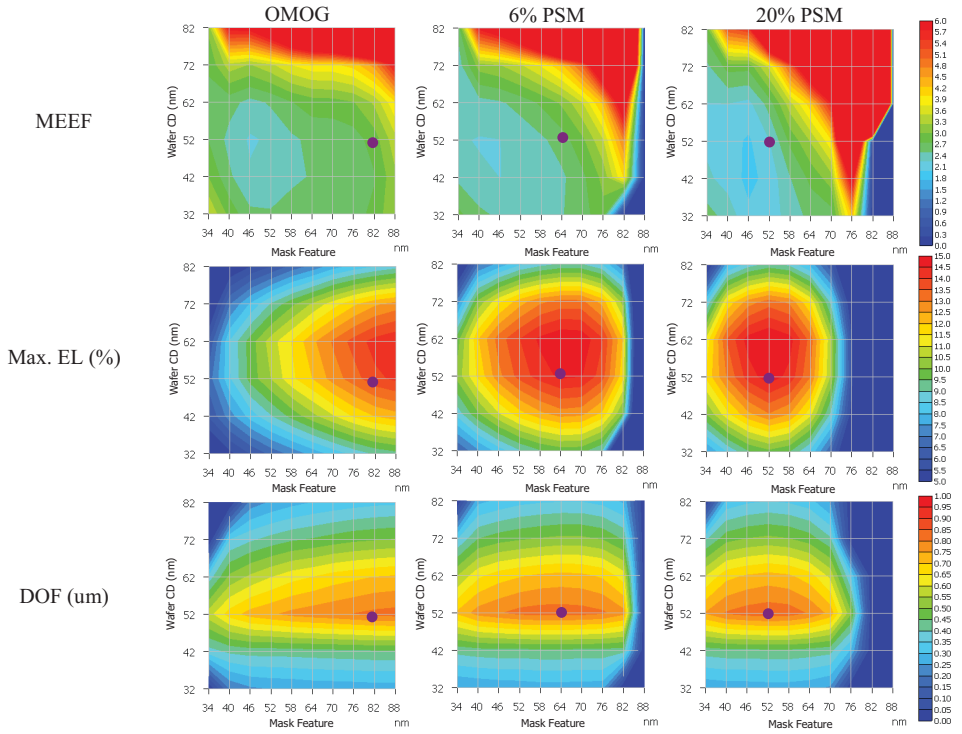

Figure 4 MEEF, max. EL and DOF through mask feature on hp 32nm in bright field: dots represent optimized mask feature.

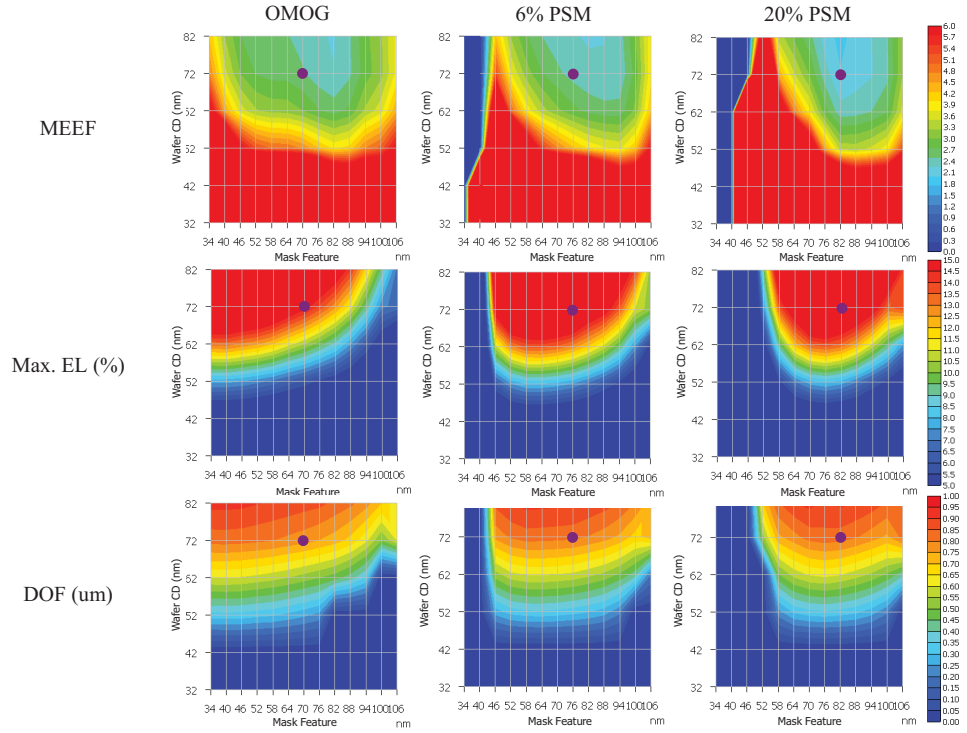

Figure 5 MEEF, max. EL and DOF through mask feature on hp 32nm in dark field: dots represent optimized mask feature.

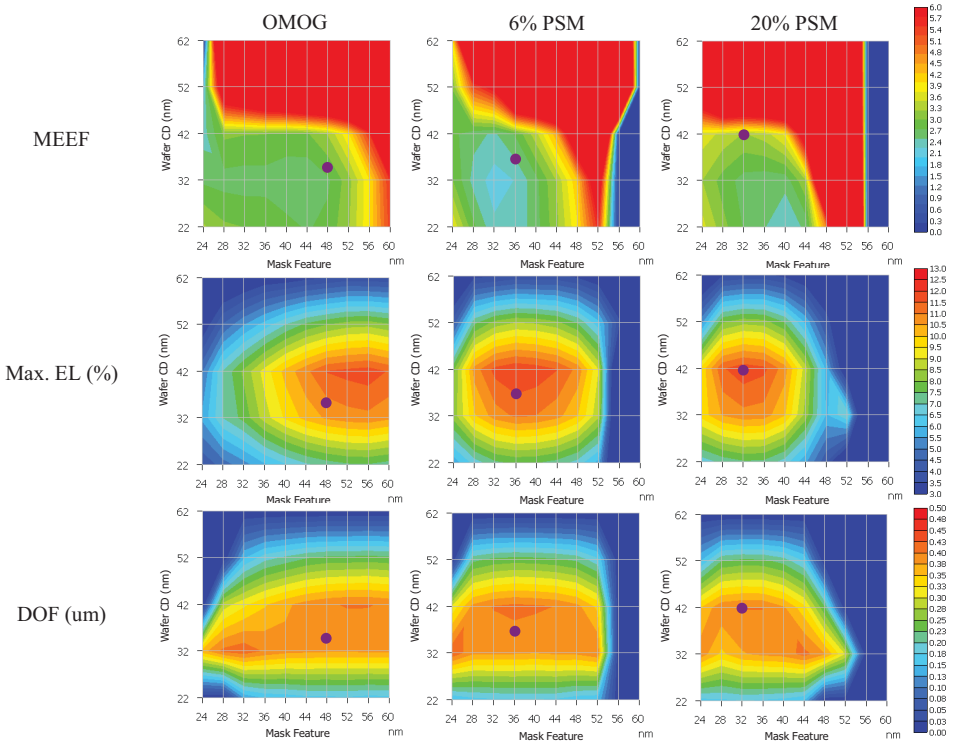

Figure 6 MEEF, max. EL and DOF through mask feature on hp 22nm in bright field: dots represent optimized mask feature.

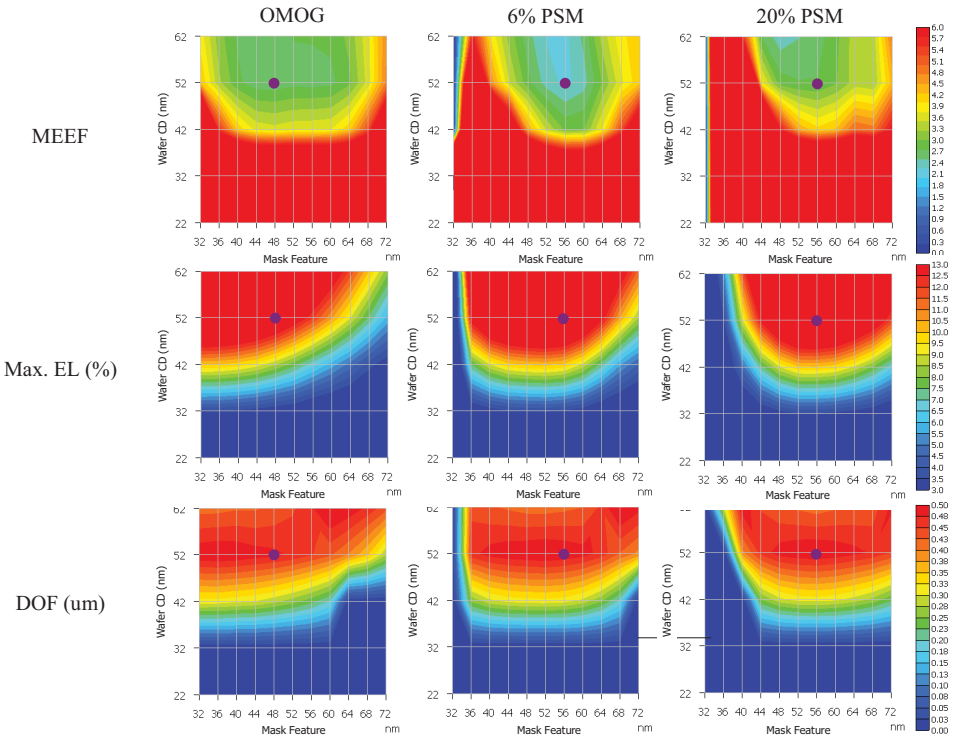

Figure 7 MEEF, max. EL and DOF as through mask feature on hp 22nm in dark field: dots represent optimized mask feature.

3.4 Lithographic performance

Figure 8 shows duty cycle of each hp for bright field and dark field. The order of higher DC for bright field features was OMOG, 6% att. PSM and 20% att. PSM. On the contrary, the order in dark field was 20% att. PSM, 6% att. PSM and OMOG. DC of OMOG was around 50% except hp 60nm in both bright field and dark field and hp 32nm in bright field.

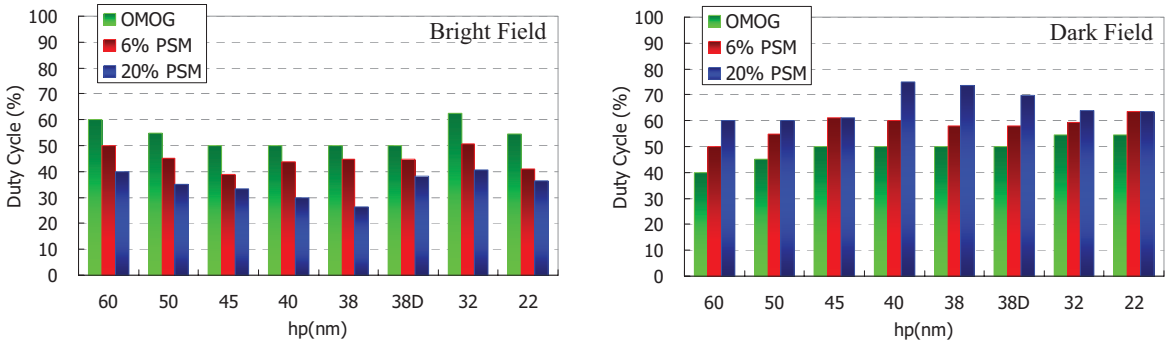

Figure 8 Duty Cycle: 38D represents hp 38nm with dipole illumination.

MEEF is shown in Figure 9. MEEF of hp 38nm with cQuad illumination is very large. Even with dipole illumination, the MEEF is larger than other hp. The MEEF for the 20% att. PSM shows higher MEEF for hp 40nm and below when it is compared to the other materials. The MEEF for OMOG is comparable with 6% att. PSM across the entire range. Figure 10 shows maximum EL. Maximum EL shrinks with decreasing hp. The maximum EL for PSMs is slightly larger than for OMOG. The DOF, shown in Figure 11, is calculated based on 5% EL. The DOF differences are very small between the three masks. On the other hand, there is big difference between hp 50nm and hp 45nm due to the same NA used for both cases. We could not obtain hp 38 nm DOF with cQuad illumination. It can be said that cQuad is not practical use on hp 38nm. Contrarily, wide DOF was obtained with dipole illumination.

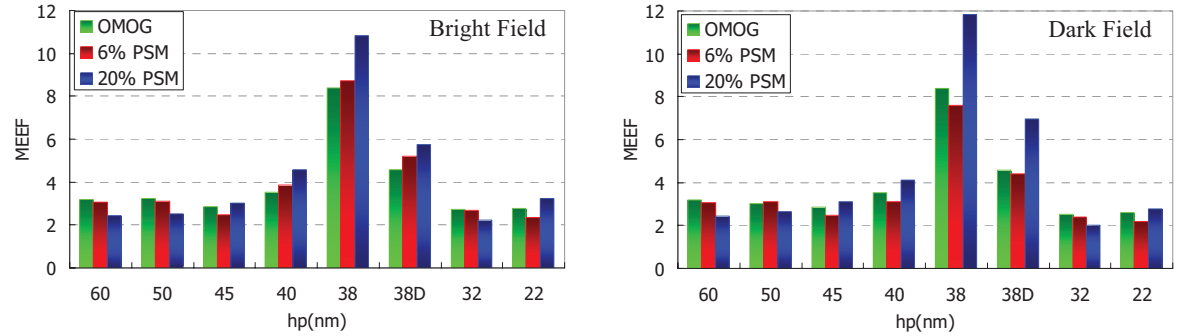

Figure 9 MEEF on various hp: 38D represents hp 38nm with dipole illumination.

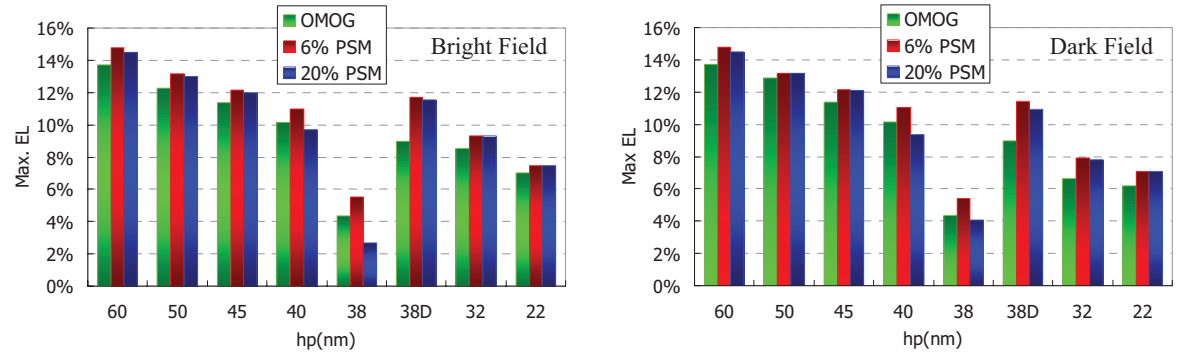

Figure 10 Maximum EL (CD±10%) on various hp: 38D represents hp 38nm with dipole illumination.

xxx

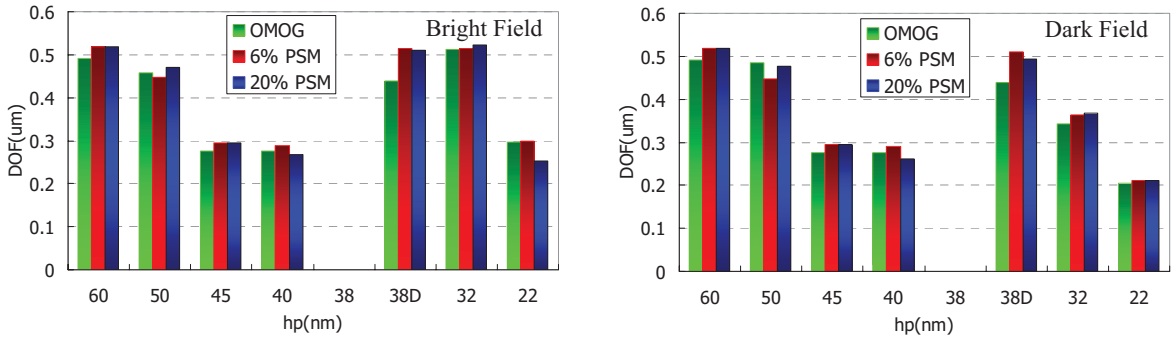

Figure 11 DOF of dense line of 5% exposure latitude on various hp: 38D represents hp 38nm with dipole illumination.

3.5 Sub Resolution Assist Feature (SRAF) width

Figure 12 shows the optimized SRAF width (4x) for an isolated pattern. In bright field, the SRAF width for OMOG is comparatively large. In spite of hp 38nm, SRAF width is larger than 60nm (15nm:1x). However, SRAF width of PSMs is less than 40nm (10nm:1x) on hp 40nm and 38nm. The small SRAF widths impact mask manufacturability. Both CD accuracy and pattern collapse during processing are concerned. It can be said that large SRAF width is benefit of OMOG. Although the required SRAF width for dark field structures is smaller for OMOG then PSM, the assist feature slots are slightly larger and are not as impacted by pattern collapse. The reason is considered that MEEF of isolated pattern with SRAF in bright field is larger than that in dark field. Large MEEF induces comparatively large SRAF width. The minimum SRAF width of OMOG in dark field is about 100nm (25nm:1x). SRAF widths in the range of 100nm (25nm:1x) are well within the current mask manufacturing capability. The DOF for an isolated pattern with SRAF is shown in Figure 13. The difference among masks is very small. If we assume DOF specs are 0.1um, DOF of hp 40nm, 38nm and 22nm is out of specs. In order to obtain enough DOF, we must optimize illumination from viewpoint of both dense pattern and isolated pattern.

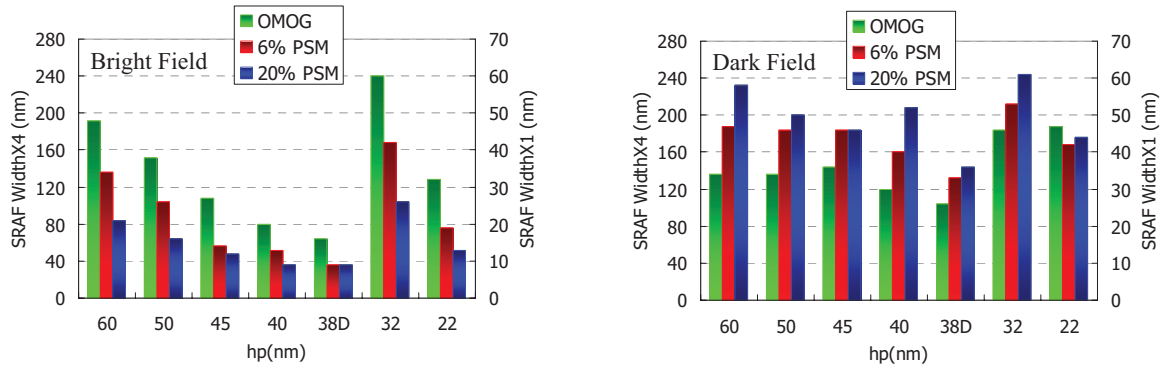

Figure 12 Optimized SRAF width on various hp: printability was evaluated within process window.

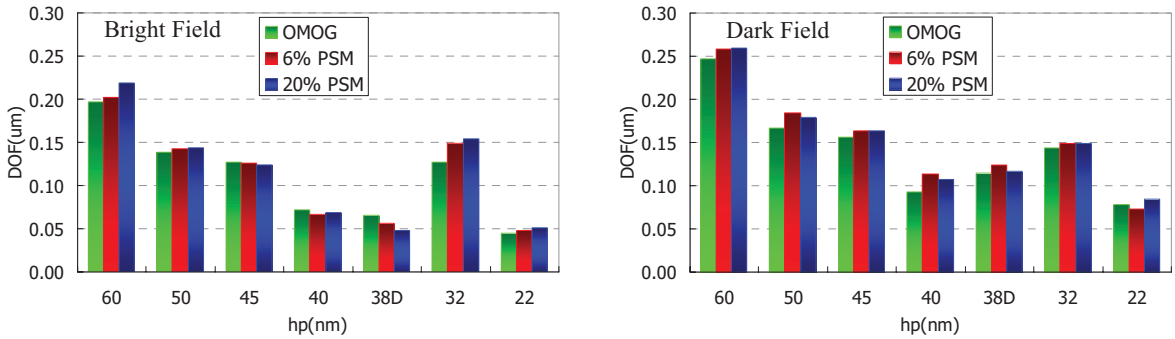

Figure 13 DOF of isolated pattern with SRAF under the condition of EL 5%.

3.6 Quartz depth variation impact

Figure 14 shows the slope of wafer CD to quartz depth. The impact to wafer CD of quartz depth variation on OMOG is very small since there is no phase restriction. However, there is a significant impact of quartz depth variation observed for PSM. This is especially true for a 20% att. PSM. Small slope of OMOG is advantageous from viewpoint of CD control on wafer.

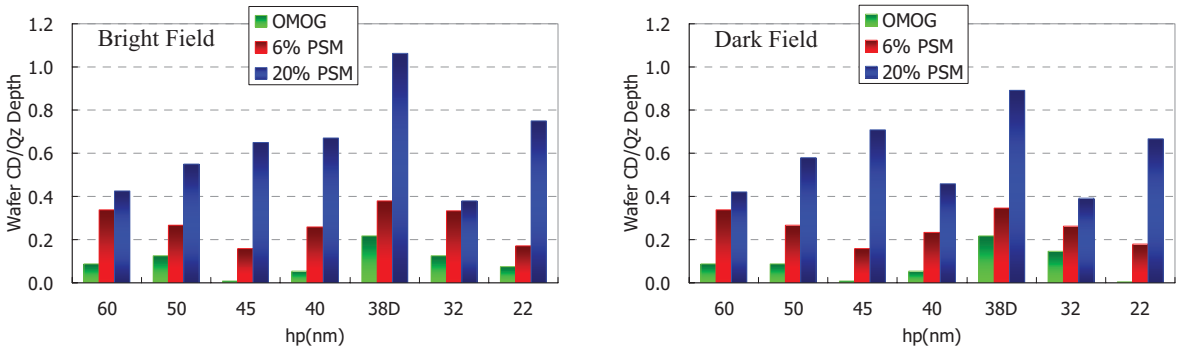

Figure 14 Quartz depth variation impact on wafer CD.

3.7 CD error on wafer

We estimated CD error on wafer caused by global mask CD error, quartz depth variation and exposure dose variation from simulation results. We assumed glolbal mask CD error is ±2nm, quartz depth variation is ±2nm and exposure dose variation is ±1%. CD error on wafer is shown in Figure 15. As a result, the difference of CD error among three masks increases with decreasing hp. The CD error observed for the 20% att. PSM is very large for 45nm hp and below. This is primarily driven by the wafer CD sensitivity to quartz depth variation. CD error of OMOG is slightly smaller than 6% att. PSM. Small wafer CD error on wafer is one of benefits of OMOG.

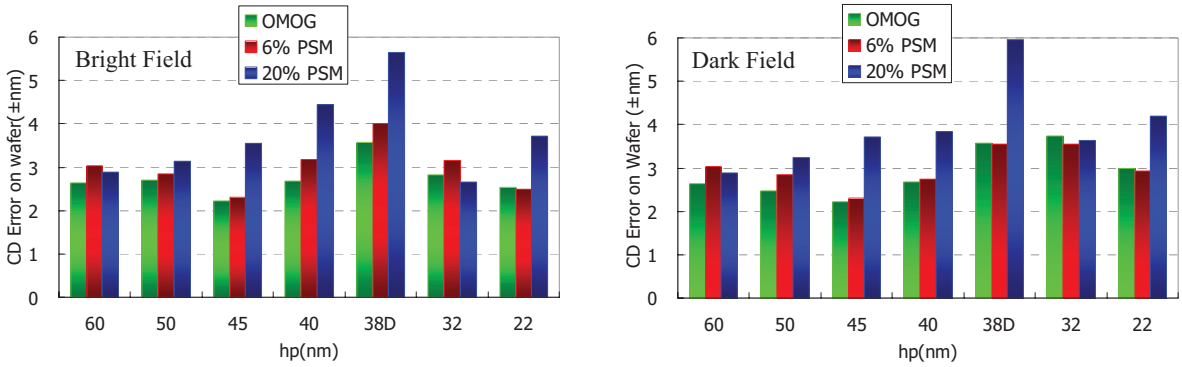

Figure 15 CD Error on wafer estimated from MEEF, quartz depth variation, and exposure dose variation.

4. EXPERIMENTAL RESULTS

Figure 16 shows MEEF and maximum EL experimental results for OMOG material for bright field features. The difference between experimental results and simulation is relatively small. Thus, we believe that our simulation accracy is high.

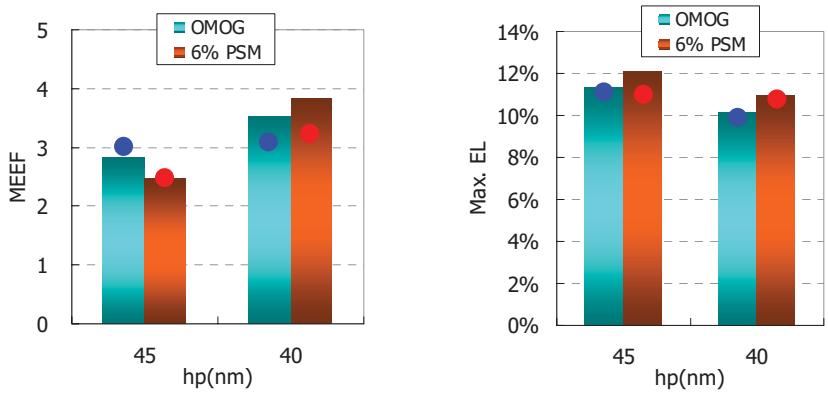

Figure 16 MEEF and maximum EL: dots represent experimental results and bars represent simulation.

We also evaluated SRAF printability for hp 45nm through pitch on wafer. Earlier we optimized the duty cycle for the hp 45nm for each material. Based on the required dose to size 45nm on wafer, we expanded our evaluation through pitch to included pitch ranges where SRAFs are required to maintain acceptable depth of focus. Figure 17 shows the wafer results for the lower duty cycle (39% DC) 6% att. PSM case, the 1:1 (50% DC) OMOG case and the 1:1 (50% DC) 6% att. PSM case. The SRAF size and mask bias was configured to target 45nm on wafer with the required dose to size. The minimum SRAF used was around 80nm at 4X.

Ealier we showed that both the 6% and 20% att. PSM show improved MEEF performance at lower duty cycles for hp 45nm bright field structures. However, when we try to expand the optimized setting through pitch for the 6% att. PSM we find that these settings result in poor SRAF printability. We also show that shifting to a higher duty cycle (50% DC) for hp 45nm improves printing performance for the 6% att PSM. However, under these conditions, we expect a higher MEEF at the minimum pitch for hp 45nm due to the negative effects from polarization. There is trade off between MEEF and SRAF printability for the att PSM. On the contrary, the OMOG gives the best combination of SRAF printability and lower MEEF.

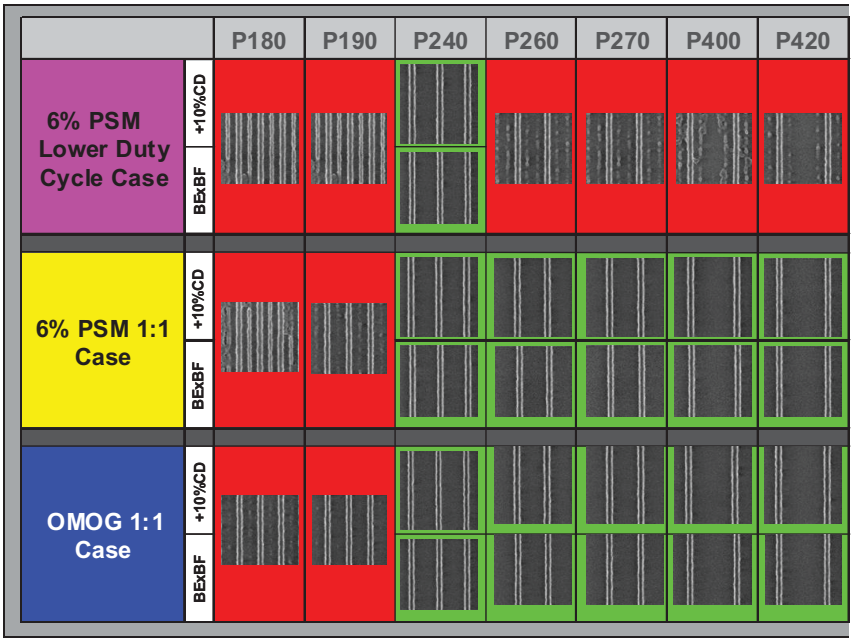

Figure 17 Experimental results of SRAF printability through pitch: red color represents that SRAF is printed, green color represents that SRAF is not printed through process window.

5. MASK CYCLE TIME

Mask cycle time continues to be a critical factor for many mask users. We estimated mask cycle time for each material in Figure 18. The cycle time for the two PSMs is comparatively larger. Especially, the cycle time of 20% att. PSM is true because of additional quartz etching. The OMOG enjoys a smaller cycle time due the shorter process procedures. Specifically a second write is required for the PSM but not for the OMOG. Moreover, OMOG benefits from reduced inspection frequency. Overall, the OMOG mask cycle time is almost 20% faster compared to the 6% att. PSM.

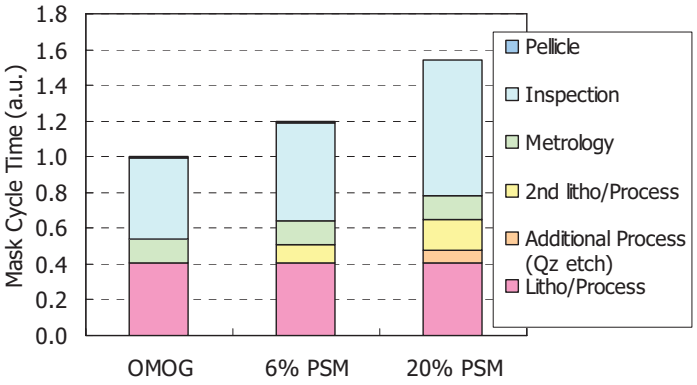

Figure 18 Manufacturing TAT: mask material OMOG, 6% att. PSM, 20% att. PSM

6. CONCLUSION

We compared lithographic performance such as MEEF, EL, DOF and SRAF printability between OMOG, 6% att. PSM and 20% att. PSM. We showed that the various materials can deliver similar lithographic performance for both bright and dark field structures for hp 45 nm and below if the mask duty cycle is optimized. However, only the OMOG delivers good lithographic performance at the densest pitches and acceptable SRAF printing at the larger pitches. An evaluation of factors that impact CD uniformity shows that the att. PSM masks are more susceptible to variations in quartz etch depth control. Finally the OMOG enjoys a 20% shorter mask cycle time due to the reduced processing content. We concluded OMOG is promising as a mask for both single exposure and double patterning in bright field and dark field.

REFERENCES

[1] International Technology Roadmap for Semiconductors 2008 Edition: Lithography.

[2] K. Adam, W. Maurer, “Polarization Effects in Immersion Lithography”, Proceedings of SPIE Vol. 5377 2004.

[3] J.Kye, G. McIntyre, Y.Norihiro, H. Levinson, “Polarization aberrations analysis in optical lithography”, Proc. SPIE Vol. 6154 2006.

[4] R. Schenker, W. Chen, G. Allen, “The MEEF NILS divergence for low k1 lithography”, Prc. SPIE 6730, 2007.

[5] T.Konishi, Y.Kojima, H.Takahashi, M.Tanabe, T.Haraguchi, M.Lamantia, Y.Fukushima, Y.Okuda, “MoSi absorber photomask for 32 nm in photomask making”, Prc. SPIE 7028, 2008.

[6] C. Mack, ”Fundamental Principles of Optical Lithography”

[7] Y.Kang, S.G.Woo,S.J.Choi, et al.,"Development of resists for thermal flow process applicable to mass production", Proc. SPIE 4345, 2001.

[8] T.Kanda, H.Tanaka, Y.Kinoshita, et al., "Adevanced microlithography process with chemical shrink technology", Proc, SPIE 3999, 2000.

[9] J. Kye, G. McIntyre, Y. Norihiro, H. Levinson, “Polarization aberration analysis in optical lithography systems”, Proc, SPIE Vol. 6154, 2006.

MAPPER: HIGH THROUGHPUT MASKLESS LITHOGRAPHY

V. Kuiper, B.J. Kampherbeek, M.J. Wieland, G. de Boer, G.F. ten Berge, J. Boers, R. Jager, T. van de Peut, J.J.M. Peijster, E. Slot, S.W.H.K. Steenbrink, T.F. Teepen, A.H.V. van Veen

MAPPER Lithography B.V., Computerlaan 15, 2628 XK Delft, The Netherlands

E-mail address: v.kuiper@mapperlithography.com

ABSTRACT

Maskless electron beam lithography, or electron beam direct write, has been around for a long time in the semiconductor industry and was pioneered from the mid-1960s onwards. This technique has been used for mask writing applications as well as device engineering and in some cases chip manufacturing. However because of its relatively low throughput compared to optical lithography, electron beam lithography has never been the mainstream lithography technology. To extend optical lithography double patterning, as a bridging technology, and EUV lithography are currently explored. Irrespective of the technical viability of both approaches, one thing seems clear. They will be expensive [1].

MAPPER Lithography is developing a maskless lithography technology based on massively-parallel electron-beam writing with high speed optical data transport for switching the electron beams. In this way optical columns can be made with a throughput of 10-20 wafers per hour. By clustering several of these columns together high throughputs can be realized in a small footprint. This enables a highly cost-competitive alternative to double patterning and EUV alternatives. In 2007 MAPPER obtained its Proof of Lithography milestone by exposing in its Demonstrator 45 nm half pitch structures with 110 electron beams in parallel, where all the beams where individually switched on and off [2].

In 2008 MAPPER has taken a next step in its development by building several tools. A new platform has been designed and built which contains a 300 mm wafer stage, a wafer handler and an electron beam column with 110 parallel electron beams. This manuscript describes the first patterning results with this 300 mm platform.

Keywords: Maskless lithography, MAPPER, exposure results

1. INTRODUCTION

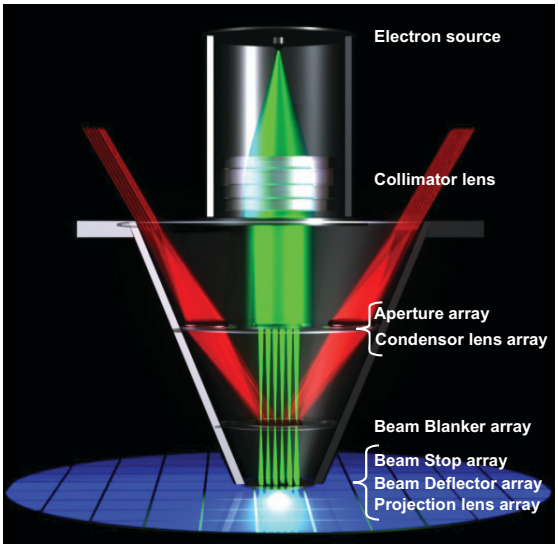

Writing time for 26 x 33 mm (incl.overhead)	2.5 sec + 2.5 sec for redundancy
Nr of beams	13,000
Gray levels	Black/white
Grid	2.25 nm
Data rate	7.5 GHz per channel
Spot size	< 25 nm
Deflection frequency	6 MHz
# of electrons per CD element	4,000
Resist sensitivity	30 μC/cm^2
Current	150 μA → 13 nA / beam
Acceleration voltage	5 kV
Stage passes per field	1
Resist	Bi / tri -layer

25th European Mask and Lithography Conference, edited by Uwe F. W. Behringer, Proc. of SPIE
Vol. 7470, 74700Q · © 2009 SPIE · CCC code: 0277-786X/09/$18 · doi: 10.1117/12.835188

Figure 1 Schematic of MAPPER's massively parallel electron beam concept

The MAPPER electron optics consists of a single high brightness cathode gun in space charge limit. An electrostatic collimator lens is used to create a collimated beam, see Figure 1. After the collimator the single beam is split up into 13,000 beams by the aperture array. After the aperture array the beamlets are focused by the condenser lens array in the intermediate focus plane. In this plane the beam blanker array is placed that can deflect each individual beam away from a clear aperture on the beam stop array to stop the electrons and switch off the beam at the wafer. After the beam stop array the beams are demagnified by the projection lens array and focused in the wafer plane. A deflector array is positioned between the beam stop array and the projection lens array to scan the beams over a range of 2 µm perpendicular to the wafer stage movement at a frequency of 6 MHz with a positioning accuracy of 1 nm.

In MAPPER's current machine the optics contains 110 electron beams and the targeted resolution is 45 nm half pitch, see Figure 2.

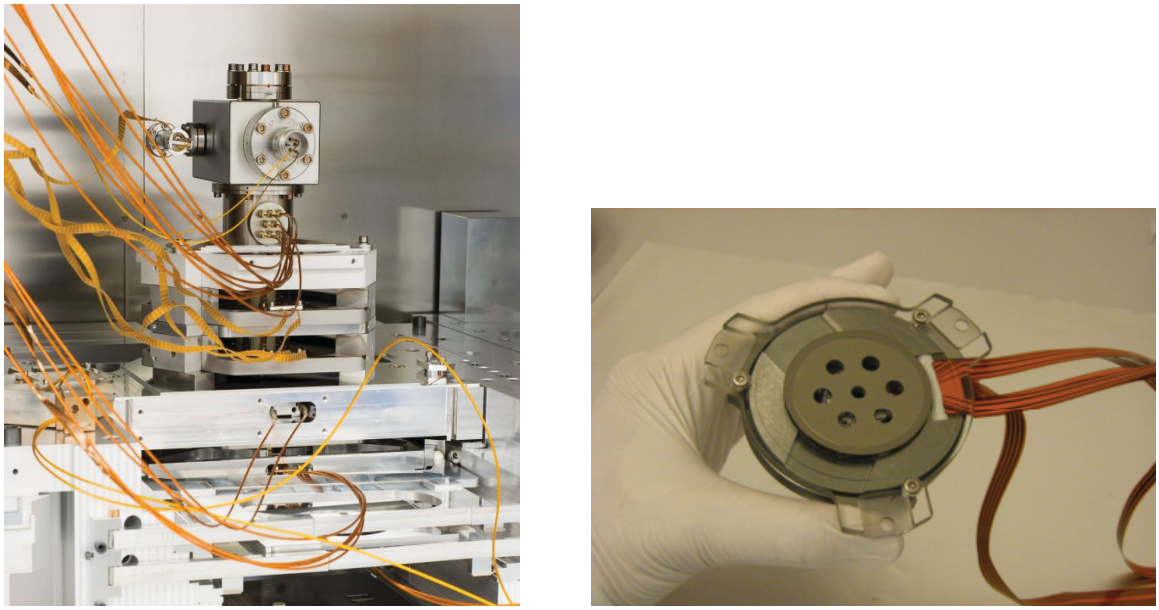

Figure 2 Overview of MAPPER's optics column (left) and an individual projection lens array (right)

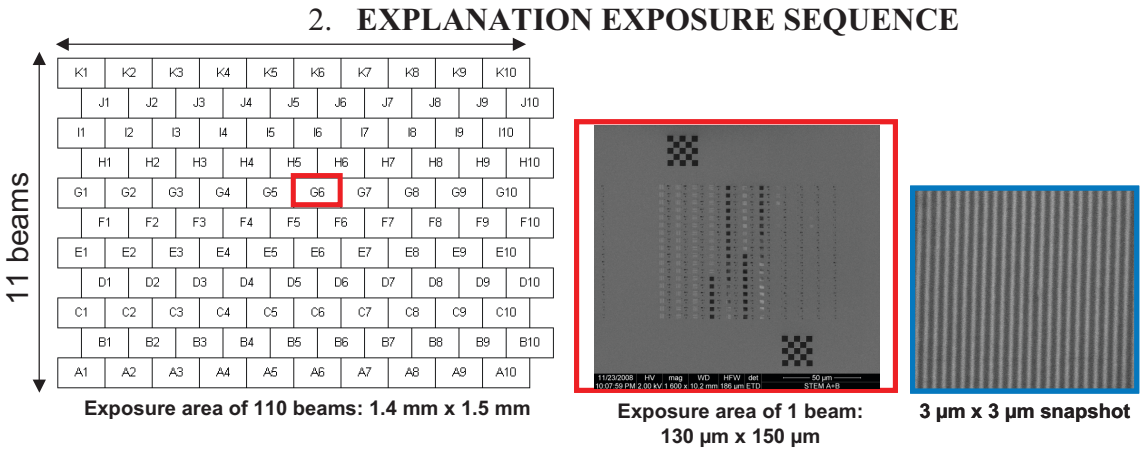

Figure 3 The arrangement of the 110 beams on the left, each exposing 130 µm x 150 µm area which is divided in 3 µm x 3 µm patterns

The exposures shown in this manuscript are static exposures. An x- and an y- deflector are used to expose 110 times an area of 3 µm x 3 µm with all the beams simultaneously. Then the wafer stage steps 5 µm to a new position and 110 new 3 µm x 3 µm areas are exposed. This is repeated 252 times resulting in 252 x 110 or 27,720 exposed patterns. Finally 110 SEM-markers are exposed. For every beam the 252 (3 µm x 3 µm) fields can contain different patterns, dose or focus settings.

The resist that is used in these exposures is 50 nm HSQ (negative) on top of a PMMA bottom layer. From Figure 4 it is clear that all beams print.

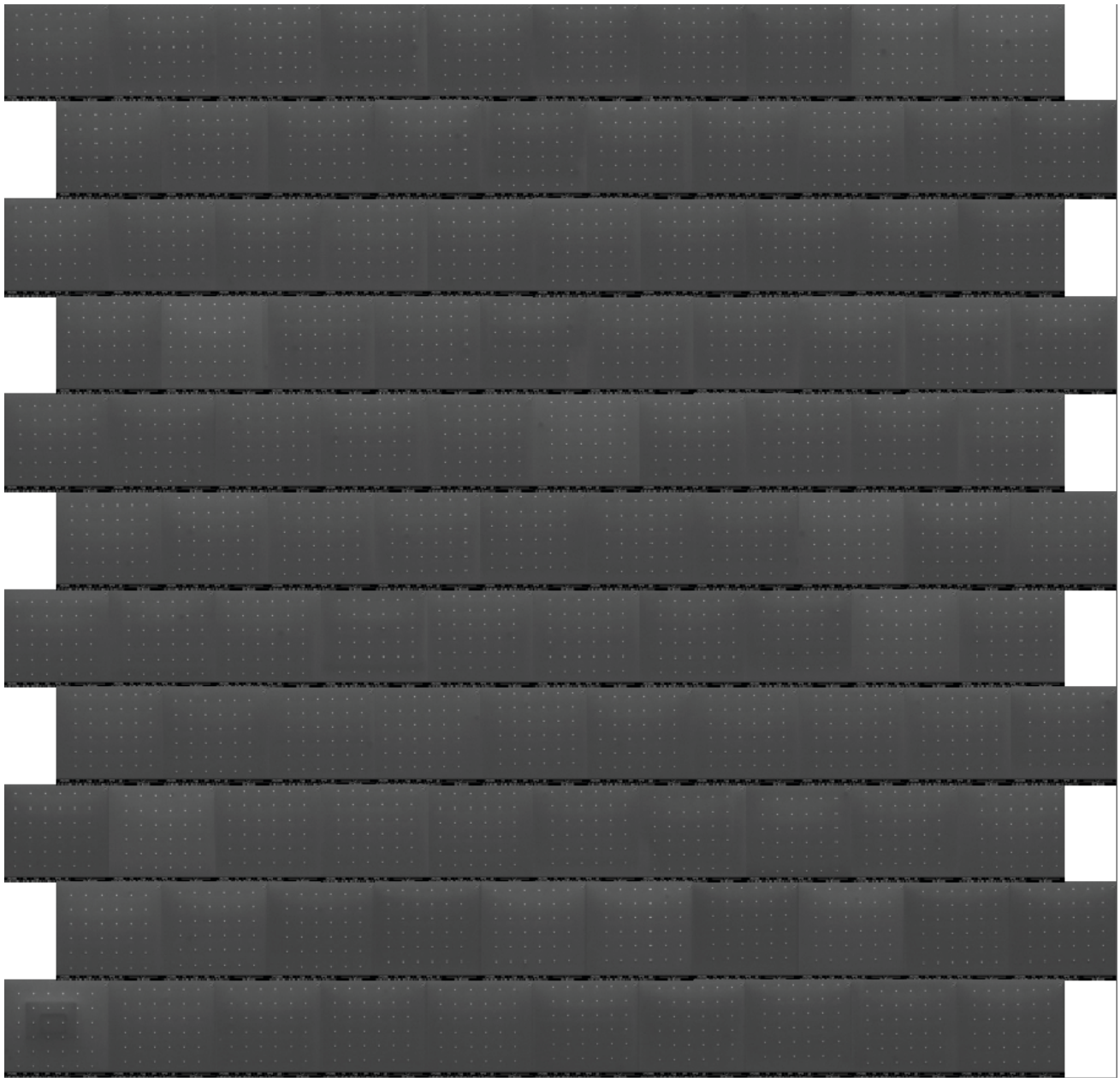

Figure 4 Overview of 110 isolated, 45 nm dot patterns exposed simultaneously

Full SEM analysis of all patterns for 110 beams is highly time consuming and therefore MAPPER has chosen for this manuscript to only inspect eleven, randomly selected beams : B2, B5, B6, B8, C2, E9, F8, G6, H2, K9 and K10.

3. EXPOSURE RESULTS

Examples of exposures are 45 nm dense lines, both horizontal and vertical lines and 45 nm dense dots. All three exposures were exposed on the same wafer.

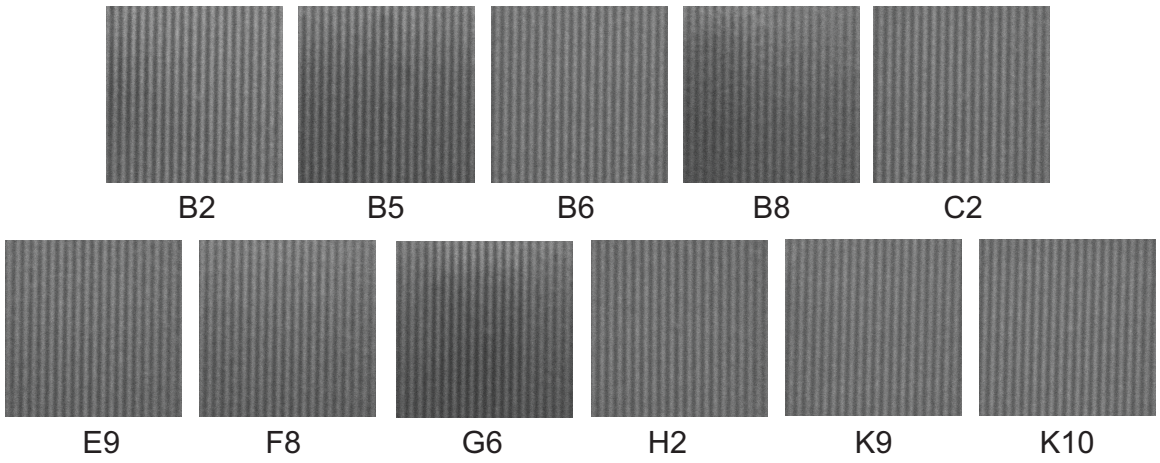

Figure 5 45 nm dense vertical lines for the eleven selected beams

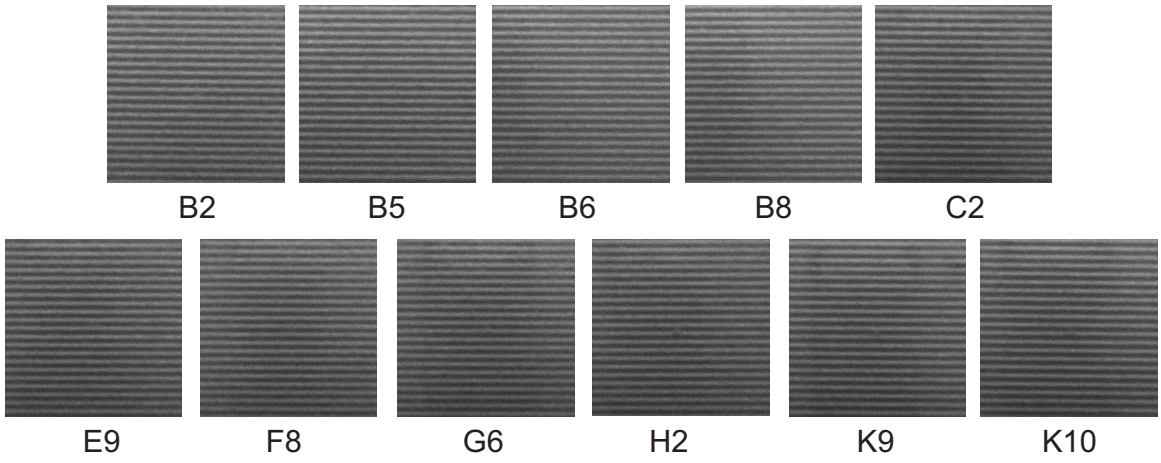

Figure 6 45 nm dense horizontal lines for the eleven selected beams

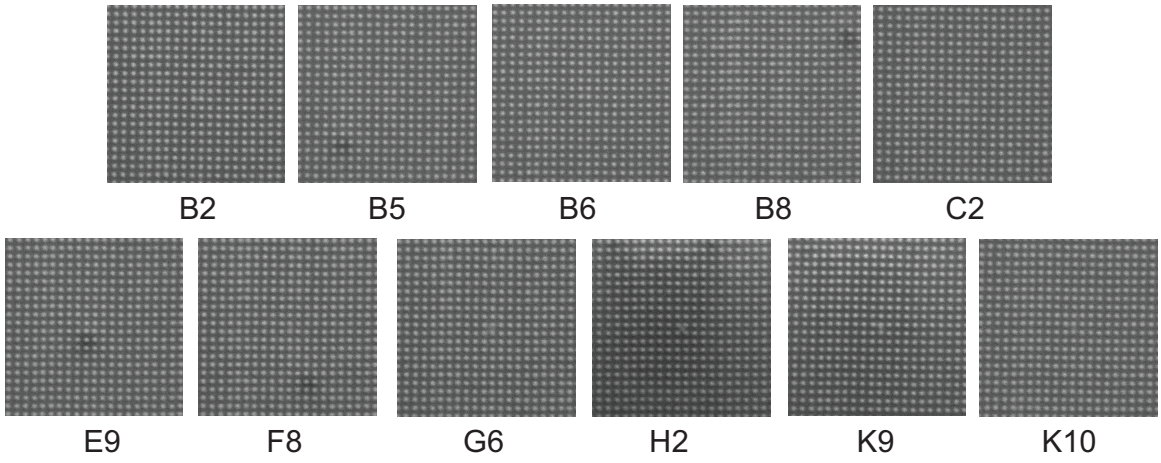

Figure 7 45 nm dense dots for the eleven selected beams

For analysis of CD/CDu, for each 3 µm x 3 µm area five 0.47 µm x 0.47 µm squares are drawn. Within each square, the line width is sampled at 3.6 nm intervals. The average of all line widths within a square is taken as the CD for that square. This results in the required 5 measurement points for each pattern. The average of the 5 measurement points is the CD for that pattern for that particular beam. The average over all 11 CD's for all beams is the CD for that pattern. The 3σ value of the 11 CD values is the CDu.

The result for the three patterns shown above is as shown in Table 1.

Table 1 Exposure analysis results

Pattern	CD [nm]		CD Mean -to-target [nm]	CDu [nm]
	Measured	Target	Measured	Measured
Dots dense	43.4	45.0	1.6	2.5
Horizontal dense	42.8	45.0	2.2	1.9
Verlines-dense	44.9	45.0	0.1	2.8

4. CONCLUSIONS

MAPPER has built its 300 mm platform based on 110 parallel electron beams in 2008. First exposures at 45 nm half pitch resolution have been performed and analyzed. On the same wafer it is observed that all beams print and based on analysis of 11 beams the CD for the different patterns iswithin 2.2 nm from target and the CD uniformity for the different patterns is better than 2.8 nm.

REFERENCES

[1] B. J. Lin, presentation Sematech Lithography workshop 2008, Bolton Landing
[2] E. Slot et al., Proc. of SPIE Vol. 6921, 69211P, (2008)